

Fullerene on Nitrogen-Adsorbed Cu(001) Nanopatterned Surfaces: From Preferential Nucleation to Layer-by-Layer Growth

Bin Lu,^{*,†} Takushi Iimori,[†] Kazuyuki Sakamoto,[‡] Kan Nakatsuji,[†] Federico Rosei,^{†,§} and Fumio Komori^{*,†}

Institute for Solid State Physics, University of Tokyo, Kashiwanoha 5-1-5, Kashiwa-shi, Chiba 277-8581, Japan, Graduate School of Advanced Integration Science, Chiba University, 1-33, Yayoi-cho, Inage-ku, Chiba-shi, Chiba, 263-8522 Japan, and INRS-EMT, University of Quebec, 1650 Boulevard Lionel Boulet, J3X 1S2 Varennes, Quebec, Canada

Received: January 14, 2008; Revised Manuscript Received: April 7, 2008

Nitrogen (N)-adsorbed Cu(001)- $c(2 \times 2)$ nanopatterned surfaces are used as templates to guide the growth of low-dimensional C₆₀ molecular nanostructures. At room temperature and during the initial stages of growth, C₆₀ molecules preferentially adsorb on the bare Cu regions on a partially N-covered grid surface. Subsequently, a two-dimensional molecular nanomesh is formed at low (~ 0.28 monatomic layer) C₆₀ coverages. Further deposition leads to C₆₀ growth on the $c(2 \times 2)$ -N surface until the first molecular layer is completed. For a N-saturated surface with trench structures, the $\langle 010 \rangle$ steps of these structures serve as initial anchoring sites for C₆₀ growth. From there, the growth proceeds two-dimensionally until a single C₆₀ layer is achieved due to island coalescence. In contrast, no nucleation site was observed when the $\langle 110 \rangle$ steps were predominant on the surface. At least up to 6 monatomic layers, the growth proceeds layer-by-layer (i.e., the overlayer morphologies are directed by the underlying substrate pattern). Four rotational domains are observed for the quasi-hexagonally close-packed C₆₀ overlayer with a nearest-neighbor C₆₀-C₆₀ distance of 1.02 nm. It was found that the interaction between C₆₀ and the $c(2 \times 2)$ -N surface is fairly weak, likely dominated by van der Waals forces, whereas the C₆₀-Cu interface is chemisorbed. Site-specific electronic effects between these two regions can be resolved by STM even for thick films.

Introduction

The potential use of molecular nanostructures in nanoelectronics has fueled effort and interest in the adsorption properties and self-assembly of molecules on solid substrates.^{1–12} In particular, the controlled self-assembly of molecular nanostructures, both for fundamental research and future applications, remains a challenge. One of the methods to control self-assembly is the use of suitably designed functional groups in the molecular structure, which are able to participate in direct noncovalent interactions among the molecules.⁴ However, the limitation and complexity of exploiting functional groups make it restrictive.

The use of specific adsorbate–substrate interactions on template surfaces is a promising and general approach to control and guide the fabrication of large-scale inorganic or organic nanostructures. The use of surface cues to guide adsorption processes¹³ has been demonstrated on a variety of spontaneously nanostructured substrates such as dislocation networks,⁶ vicinal surfaces,⁷ self-ordered biphasic systems,^{14,15} and so on. Molecular assembly on crystal surfaces is determined by a delicate balance between adsorbate–adsorbate and adsorbate–substrate interactions.¹² Ordered nanostructure arrays and thin films with distinct physical and chemical properties can be achieved on host templates by the site-specific nucleation of adsorbates and successive organized growth. Among self-organized nanotemplates, we propose using the complex patterns of the Cu(001) $c(2$

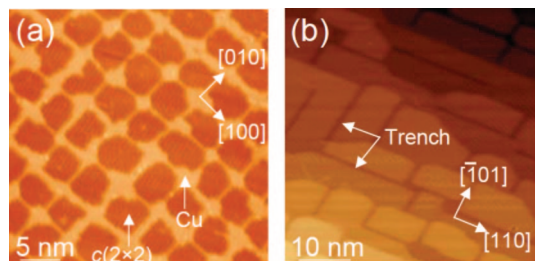


Figure 1. STM images of the N–Cu(001) nanopatterned surface: (a) 35 nm \times 35 nm area showing the typical 2D square lattice of nitrogen islands (grid surface) with ~ 0.35 ML nitrogen coverage ($V_s = 0.3$ V, $I = 0.15$ nA). (b) 50 nm \times 50 nm area showing the N-saturated surface with trench structures corresponding to 0.5 ML nitrogen coverage ($V_s = 0.6$ V, $I = 0.15$ nA).

$\times 2)$ -N^{16,17} surfaces, which have been used as templates for the controlled growth of several metal–nanoisland arrays.^{14,15,18} The directed assembly of molecular nanostructures on this nanopatterned template has not been investigated thus far.

Fullerene molecules have attracted considerable interest since their discovery because of their unique molecular structure and fascinating physical and chemical properties. The adsorption of C₆₀ on metal^{7,19–37} or semiconductor surfaces^{23,38–44} has been studied extensively using a variety of experimental techniques. Charge transfer occurs commonly at C₆₀–metal interfaces, affecting the geometrical and electronic properties of the overlayers. Hence, detailed investigations of the nucleation and growth behavior and of the bonding configurations of C₆₀ molecules on nanopatterned templates are desirable and will help better understand as to how the nanostructured templates

* Corresponding authors. E-mail: (B.L.) phylu@issp.u-tokyo.ac.jp and (F.K.) komori@issp.u-tokyo.ac.jp.

[†] University of Tokyo.

[‡] Chiba University.

[§] University of Quebec.

modify the self-organized growth and may tailor the properties of the molecular nanostructures.

In the present study, we combined the template character of Cu(001) $c(2 \times 2)$ -N surfaces with the property of C₆₀ to form pattern-guided fullerene nanostructures. We fabricated a two-dimensional (2D) molecular nanomesh, which follows the square lattice of the template. Thicker C₆₀ films with nanopatterns directed by the templates also were formed. The detailed nucleation and growth behavior, interface interactions, thermal stability, as well as electronic properties were systematically studied by in situ STM.

Experimental Procedures

The STM (Rastroscope, Denmark) measurements were performed at room temperature (RT) in an ultrahigh vacuum (UHV) chamber with a base pressure of $<9 \times 10^{-11}$ Torr. The Cu(001) surface was cleaned by several cycles of Ar⁺ ion sputtering and 800 K annealing. The cleanliness of the surface was monitored by STM and Auger electron spectroscopy (AES). Well-ordered nitrogen-adsorbed surfaces were prepared by N⁺ ion bombardment at 500 eV followed by annealing to 590–620 K for 3 min. The bombardment duration was adjusted to obtain grid (partially N-covered) and N-saturated surfaces.^{16,17} Commercially available C₆₀ in powder form (99.9%) was evaporated from a Knudsen-cell type evaporator with a deposition rate of 0.02 monolayer (ML)/min onto the nitrogen-adsorbed substrates at RT. The preparation and purification of C₆₀ are described in

ref 45. Here, one ML coverage is defined as corresponding to a single complete close-packed layer of the molecules observed with STM. Images by STM were recorded in a constant-current mode. The orthogonality of all STM images in the present paper was retrieved after correction of distortion caused by thermal drift. The image size was calibrated using an atomic image of the N-adsorbed Cu(001) surface. The error of the calibration was $\sim 4\%$.

Results and Discussion

Grid Surface. A two-dimensional square lattice of nitrogen-adsorbed areas with a typical lateral dimension of roughly 5 nm appeared when the average density of adsorbed nitrogen atoms on Cu(001) was 35% of that of the surface Cu atoms, as shown in Figure 1a¹⁶. The nitrogen-adsorbed areas are periodically separated by narrow strips of the clean Cu surface. Nitrogen atoms adsorb on the 4-fold hollow site on Cu(001), resulting in the Cu(001) $c(2 \times 2)$ -N phase, which is imaged as depressed patches with sides running along $\langle 010 \rangle$ azimuth orientations. The self-ordering of this system is driven by long-range elastic energy minimization.^{16,17} We call this self-organized nanopatterned surface the grid surface hereafter.

Figure 2a shows the morphology after deposition of ~ 0.08 ML of C₆₀ molecules onto the grid surface at RT. As expected, the fullerenes tended to selectively adsorb on the clean Cu regions due to the relatively stronger interaction between C₆₀ and Cu,^{19–22} at which charge transfer from substrate to C₆₀ is

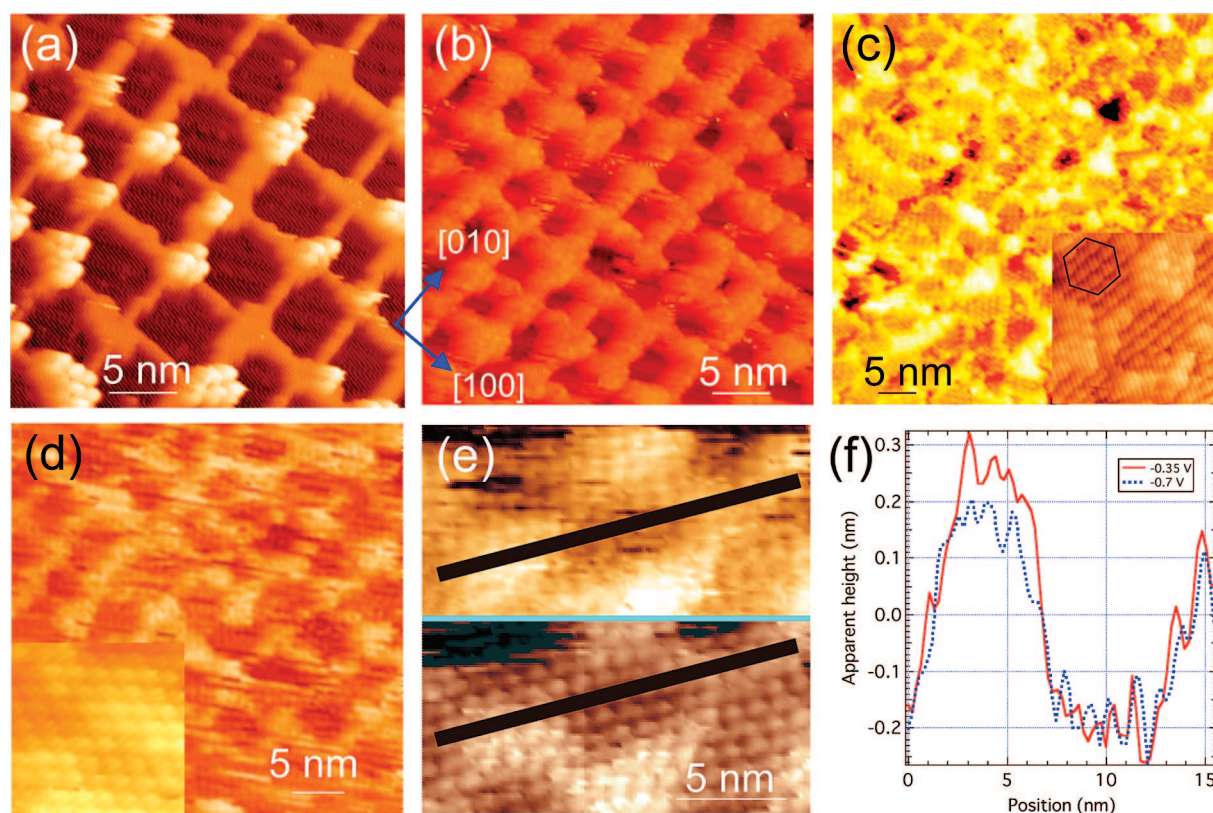


Figure 2. (a–d) STM images showing morphology evolution after RT deposition of C₆₀ on the grid surface: (a) 0.08 ML (25 nm \times 25 nm, $V_s = 0.5$ V, $I = 0.15$ nA); adsorbed C₆₀ molecules selectively nucleate on the clean Cu area. (b) ~ 0.28 ML (35 nm \times 35 nm, $V_s = 0.5$ V, $I = 0.15$ nA); 2D molecular nanomesh is formed. (c) ~ 0.95 ML (50 nm \times 50 nm, $V_s = -0.5$ V, $I = 0.15$ nA); single wetting layer is nearly completed. The imaging contrast between the two species (Cu grid area and N-covered island area) is caused by electronic effects. The inset ($V_s = -0.3$ V, $I = 0.15$ nA) shows an intermolecular resolution image of a local area with a quasi-hexagonally close-packed structure. A hexagon is overlapped on the image. (d) 3 ML (33 nm \times 33 nm, $V_s = -0.7$ V, $I = 0.18$ nA), nearly flat film. The grid pattern can still be revealed by STM. Inset: Image with the same tunneling conditions shows individual C₆₀ molecules of the top layer, which form a distorted hexagonal structure. (e) High resolution STM images for the 3 ML film with two values of V_s ; V_s for the upper portion is -0.35 V and the lower portion -0.7 V. (f) Line profiles along the lines in panel e.

reported and chemical bonding is assigned. No nucleation was observed for C₆₀ at the $c(2 \times 2)$ surface. Thus, the preferential nucleation indicates a weaker interaction of the molecule with the $c(2 \times 2)$ -N domain than with the clean Cu surface. Deposited C₆₀ can migrate freely on the $c(2 \times 2)$ area at RT. Selective nucleation on this nanopatterned surface was previously reported for the deposition of various metals and is expected to be a fairly general behavior.^{14,15,18}

An increase of C₆₀ coverage to ~ 0.28 ML naturally leads to the saturated adsorption of C₆₀ on clean Cu areas forming a 2D C₆₀ molecular nanomesh with a single molecular layer height as shown in Figure 2b. This 2D nanomesh follows the grids of the template and thus is highly regular. Further deposition gives rise to the growth of C₆₀ on the $c(2 \times 2)$ -N surface until the first molecular layer is completed. This growth behavior is clearly demonstrated in Figure 2c for a coverage approaching 1 ML. The growth of C₆₀ on this nanopatterned surface is different from metal growth on the same surface; in this case, metal nanoislands grow up to 2 ML on the grid without wetting the $c(2 \times 2)$ -N surface.^{14,15}

The apparent imaging height of the molecular film is dependent on the substrate species. In the tunneling condition shown in Figure 2c, molecules on the grid areas are imaged higher than those on the N-covered surface. This could be attributed to the combination of two possible effects: (i) geometric effect, that is, in the grid area, the initial adsorption of C₆₀ is likely buckled due to spatial constriction, resulting in height variation between the two species after a single layer is completed and (ii) electronic effect (density of states), which is evidenced by the observation of contrast change as a function of bias voltage (not shown). The latter should be the major origin for the imaging height variation between the two species. When C₆₀ adsorbed on the bare Cu mesh, interface charge transfer from Cu to C₆₀ caused the molecular orbital overlap and hybridization with substrate valence bands and influenced the electronic properties of the C₆₀ overlayer in the grid areas. On the other hand, as discussed in the next section, the interaction between C₆₀ and $c(2 \times 2)$ -N surface is a van der Waals type of interaction, and the electronic states of adsorbed C₆₀ are almost the same as those of the isolated C₆₀ molecule. Consequently, the electronic states of the C₆₀ overlayer largely depend on the substrate.

The inset in Figure 2c shows the detailed molecular arrangement of a local area, forming a quasi-hexagonally close-packed structure. Small rotational domains prevail over long-range order within the film because of the disorder of the clean Cu grids. Four rotational domains with one of the rows running nearly along either the two $\langle 110 \rangle$ or the two $\langle 100 \rangle$ directions (i.e., mutually rotated by 45°) are observed for both this surface and for the N-saturated surface. The nearest-neighbor lateral distances in all domains are in the range of 1.02 ± 0.04 nm, roughly 4 times that of the substrate Cu(001) lattice and close to an intermolecular distance of 1.002 nm in the close-packed plane of a C₆₀ fcc crystal. The same structure was widely observed in the growth of C₆₀ on various substrates,^{6,8,20,30,33} where molecule–molecule interactions prevail over molecule–substrate interactions.

We could not obtain an intramolecular image of the C₆₀ molecule on the N-adsorbed grid Cu(001) surface. It is likely that C₆₀ on the nitrogen-covered area is rotating at RT because this surface is fairly inert and the interaction between C₆₀ and underlying substrate is weak. As for C₆₀ on bare Cu, unfortunately, there are few studies available discussing the C₆₀ adsorption orientation or geometry at RT. In the study of C₆₀

on the clean Cu(001) surface, Abel et al.²⁰ discussed the coupling of C₆₀ for a heat-treated film and showed two fixed adsorption orientations, while nothing was obtained on a film without thermal treatment. Thus, whether the orientation of C₆₀ on Cu at RT is fixed is not clear at present. Moreover, in the initial growth on the grid surface, a disordered adsorption orientation and geometry can be expected for C₆₀, which arrives at the spatially constrained grid mesh.

Thicker fullerene films with ordered structures are easily achieved by further deposition at RT. The image shown in Figure 2d reveals the surface morphology after 3 ML C₆₀ deposition. Figure 2e shows a local structure, which has a quasi-hexagonal structure similar to that observed for the first layer for two different V_s values. A disordered grid pattern is still discernible in the STM image. The observed corrugation at the surface depends on the bias voltage. The line profiles along the lines on two STM images shown in Figure 2e are depicted in Figure 2f. The corrugation observed for $V_s = -0.35$ V is larger than that for $V_s = -0.7$ V.

Geometric variation and disorder of the first C₆₀ layer in the height on the two species of the substrate, which we discussed previously, significantly affect the thick film growth. The corrugation of the first C₆₀ layer can be transferred to the surface of the multilayers. This geometric effect should be the first explanation as to why the thick films still uphold the pattern. If the pattern revealed is merely due to a topographic effect, bias-dependent contrast variation would no longer exist for thick films. However, this is not the case in the present study as shown in Figure 2f. The result indicates that the interface electronic properties of the C₆₀ monolayer in direct contact with the substrate still play a role in pattern transfer to the multilayers. In previous investigations for C₆₀ multilayers, the charge transfer between C₆₀ and metal substrate was observed to localize at the interface. Hence, the bonding properties at the interface could not be resolved in thick films because of the screening operated by the dipole field. On the other hand, in the present study, the electronic change was not abrupt at the C₆₀–grid interface. Our tentative interpretation for this observation is that substrate Cu atoms in the strained grid areas could diffuse through the film at least at the first several layers, thereby affecting the electronic properties of the surface layer. The migration of substrate Cu atoms upon C₆₀ adsorption was previously observed for C₆₀ grown on bare Cu(001).²⁰

N-Saturated Surface. The N-saturated surface was completely covered by the $c(2 \times 2)$ -N structure. There are trench-like structures with a monatomic layer depth and width of a few nanometers as shown in Figure 1b. There are two kinds of C₆₀ initial growth on fully N-covered Cu(001) surfaces with exact 0.5 ML N coverage, depending on step orientation: (i) On the surface region where the $\langle 010 \rangle$ steps dominate over the $\langle 110 \rangle$ steps, C₆₀ molecules tend to nucleate along the $\langle 010 \rangle$ step edges (Figure 3b) and form short C₆₀ single molecular chains before 2D island growth on the terraces. (ii) In contrast, on the surface area where $\langle 110 \rangle$ steps are predominant as that shown in Figure 1b, there is no distinct nucleation site for the deposited C₆₀ molecules. This is evidenced by the STM image of 0.1 ML and even of lower C₆₀ coverage, which forms a compact 2D island as shown in Figure 3c. The hexagonal arrangement of C₆₀ on the island in Figure 3b can be seen in a magnified image shown in Figure 3g. The nucleation anisotropy on the step edges may be an indication of the step energy anisotropy, and $\langle 010 \rangle$ steps could be favored for C₆₀ nucleation because they correspond to the directions of close packing of the underlying $c(2 \times 2)$ -N. Here, we note that

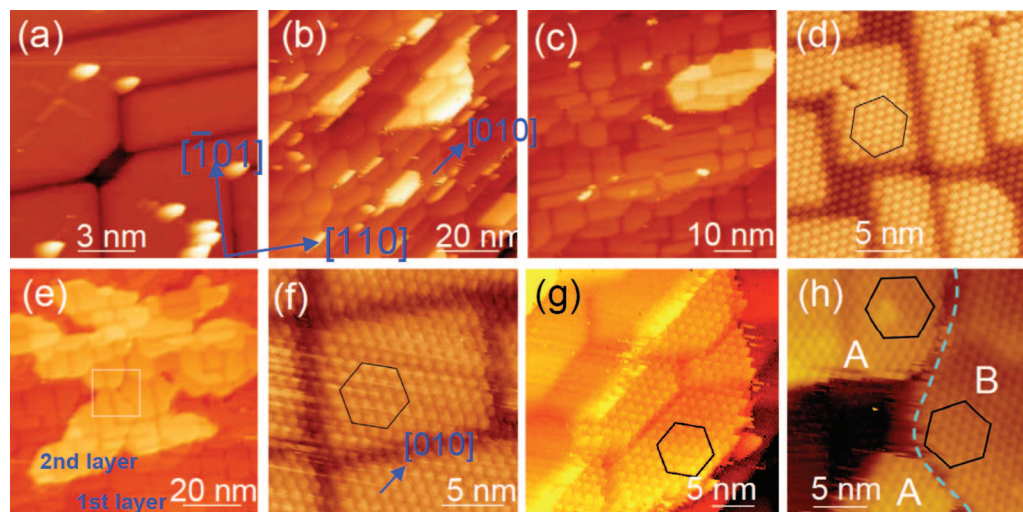


Figure 3. (a–f) STM images of morphology evolution after RT deposition of C_{60} on the N-saturated surfaces with or without defects: (a) 0.05 ML C_{60} at the surface with defects ($13 \text{ nm} \times 13 \text{ nm}$, $V_s = 1.4 \text{ V}$, $I = 0.15 \text{ nA}$). The deposited C_{60} molecules selectively adsorb at the defects sites. (b) 0.1 ML C_{60} at the area where $\langle 010 \rangle$ steps dominated ($80 \text{ nm} \times 80 \text{ nm}$, $V_s = -1 \text{ V}$, $I = 0.15 \text{ nA}$). The step edges running along the $\langle 010 \rangle$ directions can serve as initial nucleation sites. (c) 0.1 ML C_{60} at the area where $\langle 110 \rangle$ steps dominated, forming 2D molecular islands ($68 \text{ nm} \times 68 \text{ nm}$, $V_s = 0.5 \text{ V}$, $I = 0.15 \text{ nA}$), while no distinct nuclei site was observed. (d) Formation of a patterned template guided wetting layer with a distorted hexagonal structure after 1 ML C_{60} deposition ($23 \text{ nm} \times 23 \text{ nm}$, $V_s = 0.5 \text{ V}$, $I = 0.15 \text{ nA}$). The orientation of the C_{60} domain is signified by a hexagon. (e) 2D compact island formed on the second layer with ~ 1.6 ML C_{60} coverage ($85 \text{ nm} \times 85 \text{ nm}$, $V_s = 0.5 \text{ V}$, $I = 0.15 \text{ nA}$). (f) After 3 ML C_{60} deposition, proceeding the template guided layer-by-layer growth ($20 \text{ nm} \times 20 \text{ nm}$, $V_s = 0.5 \text{ V}$, $I = 0.15 \text{ nA}$). The orientation of the C_{60} domain is signified by a hexagon. (g) Magnified STM image of C_{60} monolayer domain on the $\langle 010 \rangle$ steps dominated surface. C_{60} molecules are arranged along the steps. The domain is the same as that shown at the upper right area in panel b. (h) Magnified STM image showing two C_{60} domains on the island ($V_s = 0.5 \text{ V}$, $I = 0.15 \text{ nA}$). The area shown as a white square in panel e is magnified. A domain boundary between two rotational domains (labeled as A and B) is shown as a dotted curve. Part of C_{60} at the island edges of the second layer was removed by STM after taking the image shown in panel e.

nitrogen defects, such as bare Cu regions induced by N-desorption, naturally serve as nucleation sites for C_{60} adsorbates as shown in Figure 3a.

Further deposition gives rise to the growth of C_{60} overspreading over the terraces until eventually a wetting layer is formed upon island coalescence (Figure 3d). The morphology of the C_{60} overlayer is guided by the nanopatterned template and thus exhibits the same trench-like structure as the substrate. The C_{60} molecules in Figure 3d are arranged into a distorted hexagonal structure similar to the one discussed for the grid surface. Upon close inspection, a slight distortion in the C_{60} overlayer at trench areas was consistently observed. This is reasonable because even for the template itself¹⁶ and for a MnN island superstructure on Cu(001),^{46,47} a slight lattice distortion for the topmost surface layer was observed near the trench. The four rotational domains are seen also on the N-saturated surface, and we marked the orientation of the domain in Figure 3d as a hexagon.

Figure 3e displays a morphology obtained after 1.6 ML C_{60} deposition at RT. The second layer forms a compact single-layer large island that is still directed by the substrate's nanoscale patterning. The coalescence growth mode controls the second-layer growth, and the C_{60} adsorbates on top of the first C_{60} layer tend to aggregate to form large islands rather than many small islands. The detailed arrangement of the molecules can be clearly seen in a magnified image shown in Figure 3h. A domain boundary for the second layer is labeled as a dashed line. Two 45° rotated domains marked A and B with quasi-hexagonally close-packed rows are identified as in the surface C_{60} layer. The B domain has the same orientation as that in Figure 3d. These findings suggest that the growth of a thicker C_{60} film up to this stage is subsurface guided. Actually, the C_{60} growth guided by the interface nanopattern continues at least up to 6 ML coverage. Figure 3f shows a small-scale STM image of 3 ML C_{60} on the template, where the surface morphology of the film depends

on the interface nanostructured template. The domain labeled here and the one shown in Figure 3d are mutually rotated by 45° . The multilayer film maintained the layer-by-layer assembly, at least up to 6 ML. This suggests a Frank–van der Merwe-type growth mode for C_{60} on N-saturated Cu(001). The C_{60} molecules in the surface layer of the thick film are arranged into a quasi-hexagonally close-packed structure with the nearest C_{60} – C_{60} distance close to that of the bulk (1 nm) throughout our study, and thus, the molecular overlayer possibly adopts a distorted fcc stack. One may note the discrepancy of island edges of the second layer between the large image in Figure 3e and its magnified image in Figure 3h. Part of the C_{60} was removed and displaced during the consecutive scanning of the STM tip because of the weak molecule–molecule interactions.

We also investigated the stability of molecular overlayers with respect to annealing. The thinner C_{60} film and even the original N-covered substrate can be retrieved by annealing the thicker C_{60} film on the patterned surface. Annealing of 6 ML C_{60} on N-saturated Cu(001) at 210°C for 3 min led to the desorption of C_{60} molecules with a single layer of C_{60} remaining on the patterned surface as shown in Figure 4a. Figure 4b reveals the detailed structure of the bright area in Figure 4a, exhibiting a quasi-hexagonal structure similar to the one observed before annealing. The profile A–A' crossing the small hole in Figure 4a shows an apparent height difference of 0.69 nm (see inset), close to the hard sphere diameter (0.71 nm), and thus can be interpreted as a single-layer C_{60} overlayer.⁴⁸ Moreover, the structure inside the hole was identified on the original N-covered phase by zoom-in scanning of larger holes at the same surface (not shown). This is better clarified after further annealing the sample for 5 min. The large area of the Cu(001) $c(2 \times 2)$ –N structure was recovered as presented in Figure 4c. Trenches in the $c(2 \times 2)$ –N region can be distinctly seen, indicating the good thermal stability of the template at this temperature, also

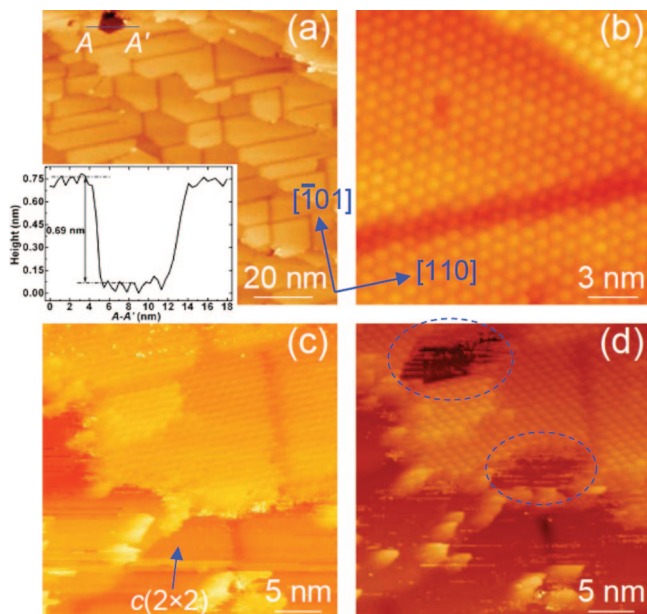


Figure 4. Thermal and structural stability of the C_{60} overlayer: (a) large-scale STM image taken after annealing the sample shown in Figure 3f at 210 °C for 3 min (100 nm \times 100 nm, $V_s = 0.5$ V, $I = 0.15$ nA). The inset shows the profile along the lines A–A', indicating a single molecular layer depth for the hole. (b) STM image revealing the detailed molecular arrangement of the bright area in panel a (18 nm \times 18 nm, $V_s = 1.5$ V, $I = 0.1$ nA). (c) STM image of the same sample after further annealing at 210 °C for 5 min (32 nm \times 32 nm, $V_s = 0.2$ V, $I = 0.2$ nA). Large area of the $c(2 \times 2)$ template surface was recovered. (d) Successive scanning at the same area as in panel c; C_{60} molecules at the dashed ellipses marked areas that disappeared after scanning the whole surface twice with the same tunneling conditions as in panel c. We propose the removal of C_{60} by tip to other areas, which is evidenced by the observation of individual molecules or small clusters on the recovered $c(2 \times 2)$ area (32 nm \times 32 nm, $V_s = 0.5$ V, $I = 0.16$ nA).

suggesting that the adsorption of C_{60} molecules does not alter the underlying substrate patterning. This observation is in contrast to the deposition of Co atoms on the $c(2 \times 2)$ –N surface, which causes N–Cu bonds to break and N atoms to segregate on the surface of the Co overlayer at RT.⁴⁹ The N-saturated substrate can be fully recovered by longer annealing at the same temperature. The observed stability of the $c(2 \times 2)$ –N structure and weak bonding between C_{60} and substrate $c(2 \times 2)$ area indicates that the C_{60} molecules are physisorbed.

It was recently reported that C_{60} molecules completely desorb from the SiC nanomesh at 200 °C,⁸ whereas desorption from the HOPG surface occurs between 237 and 257 °C,³⁴ close to the desorption temperature we found for C_{60} from the N-saturated Cu(001) surface. This type of bonding was previously assumed to be van der Waals forces for C_{60} molecules on the two surfaces (HOPG and SiC nanomesh). Thus, because of the similar desorption temperature, the interaction between C_{60} molecules and Cu(001) $c(2 \times 2)$ –N surface also can be assigned to a van der Waals force. This is different from the interaction between C_{60} molecules and clean Cu(001), on which C_{60} is chemisorbed as we discussed previously. The weak interaction between C_{60} and substrate $c(2 \times 2)$ area is further suggested from our STM study. By approaching the STM tip to the surface using a low bias, it is possible to displace several C_{60} molecules. This is demonstrated by the images shown in Figure 4c,d (note the dashed ellipse labeled areas), which were obtained at the same area. The displaced molecules are possibly transported to the tip during the approach and are moved to other areas of the

surface during scanning, for instance, to the recovered $c(2 \times 2)$ region as evidenced by the observation of individual molecules in these areas. This does not always occur using identical parameters for tunneling. It might depend on other parameters such as scanning speed and tip state, etc. We can only claim that a small tunneling resistance (< 1 Gohm) is necessary for scratching or removal of C_{60} with a STM tip.

Conclusion

The nucleation, growth behavior, and interaction of C_{60} molecules deposited onto N–Cu(001) nanopatterned surfaces at RT were observed by STM. On the partially N-covered grid surface, the adsorbed molecules diffused freely at the Cu(001) $c(2 \times 2)$ –N areas to nucleate on the clean Cu regions, forming a 2D square molecular nanomesh at low (~ 0.28 ML) C_{60} coverages. The first molecular overlayer was completed by further deposition of C_{60} growing on the $c(2 \times 2)$ surface. For an N-saturated surface without defects, preferential nucleation was observed only for the $\langle 010 \rangle$ step dominated surface. The growth of C_{60} follows a layer-by-layer regime, and the morphology of the molecular overlayer was guided by the underlying template in all cases. Quasi-hexagonally closed-packed structures with rotational domains were formed for the overlayers with molecular nearest-neighbor distances close to that in the C_{60} van der Waals crystal. On the grid surface, the apparent imaging height difference for the films observed at all coverages was tentatively attributed to a combination of electronic effects in the single-layer C_{60} overlayer and the different coupling of C_{60} molecules to the underlying substrate layer at different regions. The template $c(2 \times 2)$ –N surface can be recovered by annealing the as-grown C_{60} film at 210 °C for several minutes, and the interaction between C_{60} and substrate $c(2 \times 2)$ was assigned to a van der Waals-type force. Similarly to other templates such as SiC nanomesh⁸ and the nanograting that forms on Cu(110) upon exposure to oxygen,^{50–52} N–Cu(001) nanopatterned surfaces are promising to guide the formation of a variety of well-defined molecular nanostructures and organic films for future nanoelectronic and organic electronic devices.

Acknowledgment. This work was partly carried out by joint research at the Institute for Solid State Physics (ISSP), University of Tokyo. F.R. is grateful to ISSP, University of Tokyo for a Visiting Professorship from November 2006 to February 2007. F.R. also acknowledges FQRNT and the Canada Research Chairs program for partial financial support.

References and Notes

- (1) Barth, J. V.; Costantini, G.; Kern, K. *Nature (London)* **2005**, *437*, 671.
- (2) Rosei, F. *J. Phys.: Condens. Matter* **2004**, *16*, 1373.
- (3) Whitesides, G. M.; Mathias, J. P.; Seto, C. T. *Science (Washington, DC, U.S.)* **1991**, *254*, 1312.
- (4) Yokoyama, T.; Yokoyama, S.; Kamikado, T.; Okuno, Y.; Mashiko, S. *Nature (London)* **2001**, *413*, 619.
- (5) Corso, M.; Auwärter, W.; Muntwiler, M.; Tamai, A.; Greber, T.; Osterwalder, J. *Science (Washington, DC, U.S.)* **2004**, *303*, 217.
- (6) Ait-Mansour, K.; Ruffieux, P.; Xiao, W.; Gröning, P.; Fasel, R.; Gröning, O. *Phys. Rev. B: Condens. Matter Mater. Phys.* **2006**, *74*, 195418.
- (7) Xiao, W.; Ruffieux, P.; Ait-Mansour, K.; Gröning, O.; Palotas, K.; Hofer, W. A.; Gröning, P.; Fasel, R. *J. Phys. Chem. B* **2006**, *110*, 21394.
- (8) Chen, W.; Zhang, H. L.; Xu, H.; Tok, E. S.; Loh, K. P.; Wee, A. T. S. *J. Phys. Chem. B* **2006**, *110*, 21873.
- (9) Pedersen, M. Ø.; Murray, P. W.; Lægsgaard, E.; Stensgaard, I.; Besenbacher, F. *Surf. Sci.* **1997**, *389*, 300.
- (10) Kröger, J.; Néel, N.; Jensen, H.; Berndt, R.; Rurali, R.; Lorente, N. *J. Phys.: Condens. Matter* **2006**, *18*, 51.
- (11) Rosei, F.; Schunack, M.; Jiang, P.; Gourdon, A.; Lægsgaard, E.; Stensgaard, I.; Joachim, C.; Besenbacher, F. *Science (Washington, DC, U.S.)* **2002**, *296*, 328.

- (12) Rosei, F.; Schunack, M.; Naitoh, Y.; Jiang, P.; Gourdon, A.; Laegsgaard, E.; Stensgaard, I.; Joachim, C.; Besenbacher, F. *Prog. Surf. Sci.* **2003**, *71*, 95.
- (13) Cicoira, F.; Rosei, F. *Surf. Sci.* **2006**, *600*, 1.
- (14) Matsumoto, Y.; Tanaka, K. *Jpn. J. Appl. Phys.* **1998**, *37*, 154.
- (15) Komori, F.; Ohno, S.; Nakatsuji, K. *Prog. Surf. Sci.* **2004**, *77*, 1.
- (16) Leiblsle, F. M.; Flipse, C. F. J.; Robinson, A. W. *Phys. Rev. B: Condens. Matter Mater. Phys.* **1993**, *47*, 15865.
- (17) Driver, S. M.; Woodruff, D. P. *Surf. Sci.* **2001**, *492*, 11.
- (18) Rousset, S.; Croset, B.; Girard, Y.; Prévot, G.; Repain, V.; Rohart, S. *Crit. Rev. Phys. Phys.* **2005**, *6*, 33.
- (19) Rowe, J. E.; Rudolf, P.; Tjeng, L. H.; Malic, R. A.; Meigs, G.; Chen, C. T.; Chen, J.; Plummer, E. W. *Int. J. Mod. Phys. B* **1992**, *6*, 3909.
- (20) Abel, M.; Dmitriev, A.; Fasel, R.; Lin, N.; Barth, J. V.; Kern, K. *Phys. Rev. B: Condens. Matter Mater. Phys.* **2003**, *67*, 245407.
- (21) Dutton, G.; Zhu, X.-Y. *J. Phys. Chem. B* **2004**, *108*, 7788.
- (22) Tsuei, K.-D.; Johnson, P. D. *Solid State Commun.* **1997**, *101*, 337.
- (23) Weaver, J. H.; Hauffer, R. E.; Smalley, R. E. *Phys. Rev. B: Condens. Matter Mater. Phys.* **1991**, *44*, 13747.
- (24) Altman, E. I.; Colton, R. J. *Phys. Rev. B: Condens. Matter Mater. Phys.* **1993**, *48*, 18244.
- (25) Mayuyama, Y.; Ohno, K.; Kawazoe, Y. *Phys. Rev. B: Condens. Matter Mater. Phys.* **1995**, *52*, 2070.
- (26) Johansson, M. K.-J.; Maxell, A. J.; Gray, S. M.; Brühwiler, P. A.; Mancini, D. C.; Johansson, L. S. O.; Mårtensson, N. *Phys. Rev. B: Condens. Matter Mater. Phys.* **1996**, *54*, 13472.
- (27) Cepek, C.; Goldoni, A.; Modesti, S. *Phys. Rev. B: Condens. Matter Mater. Phys.* **1996**, *53*, 7466.
- (28) Hunt, M. R. C.; Rudolf, P.; Modesti, S. *Phys. Rev. B: Condens. Matter Mater. Phys.* **1997**, *55*, 7882.
- (29) Tsuei, K.-D.; Yuh, J.-Y.; Tzeng, C.-T.; Chu, R.-Y.; Chung, S.-C.; Tsang, K.-L. *Phys. Rev. B: Condens. Matter Mater. Phys.* **1997**, *56*, 15412.
- (30) Murray, P. W.; Pedersen, M. Ø.; Lægsgaard, E.; Stensgaard, I.; Besenbacher, F. *Phys. Rev. B: Condens. Matter Mater. Phys.* **1997**, *55*, 9360.
- (31) Tzeng, C.-T.; Lo, W.-S.; Yuh, J.-Y.; Chu, R.-Y.; Tsuei, K.-D. *Phys. Rev. B: Condens. Matter Mater. Phys.* **2000**, *61*, 2263.
- (32) Grobis, M.; Lu, X.; Crommie, M. F. *Phys. Rev. B: Condens. Matter Mater. Phys.* **2002**, *66*, 161408.
- (33) Rogero, C.; Pascual, J. I.; Gómez-Herrero, J.; Baró, A. M. *J. Chem. Phys.* **2002**, *116*, 832.
- (34) Reinke, P.; Feldemann, H.; Oelhafen, P. *J. Chem. Phys.* **2003**, *119*, 12547.
- (35) Pai, W. W.; Hsu, C.-L. *Phys. Rev. B: Condens. Matter Mater. Phys.* **2003**, *68*, 121403.
- (36) Yuan, L.-F.; Yang, J.; Wang, H.; Zeng, C.; Li, Q.; Wang, B.; Hou, J. G.; Zhu, Q.; Chen, D. M. *J. Am. Chem. Soc.* **2003**, *125*, 169.
- (37) Silien, C.; Pradhan, N. A.; Ho, W.; Thiry, P. A. *Phys. Rev. B: Condens. Matter Mater. Phys.* **2004**, *69*, 115434.
- (38) Yao, X.; Workman, R. K.; Peterson, C. A.; Chen, D.; Sarid, D. *Appl. Phys. A: Mater. Sci. Process.* **1998**, *66*, 107.
- (39) Hou, J. G.; Yang, J. L.; Wang, H. Q.; Li, Q. X.; Zeng, C. G.; Lin, H.; Wang, B.; Chen, D. M.; Zhu, Q. S. *Phys. Rev. Lett.* **1999**, *83*, 3001.
- (40) Pascuala, J. I.; Gómez-Herrero, J.; Rogero, C. J.; Baró, A. M.; Sánchez-Portal, D.; Artacho, E.; Ordejón, P.; Soler, J. M. *Chem. Phys. Lett.* **2000**, *321*, 78.
- (41) Dunn, A. W.; Svensson, E. D.; Dekker, C. *Surf. Sci.* **2001**, *498*, 237.
- (42) Moriarty, P.; Upward, M. D.; Dunn, A. W.; Ma, Y.-R.; Beton, P. H.; Teehan, D. *Phys. Rev. B: Condens. Matter Mater. Phys.* **1998**, *57*, 362.
- (43) Sakamoto, K.; Harada, M.; Kondo, D.; Kimura, A.; Kakizaki, A.; Suto, S. *Phys. Rev. B: Condens. Matter Mater. Phys.* **1998**, *58*, 13951.
- (44) Cepek, C.; Schiavuta, P.; Sancrotti, M.; Pedio, M. *Phys. Rev. B: Condens. Matter Mater. Phys.* **1999**, *60*, 2068.
- (45) Sakamoto, K.; Suzuki, T.; Harada, M.; Wakita, T.; Suto, S.; Kasuya, A. *Phys. Rev. B: Condens. Matter Mater. Phys.* **1998**, *57*, 9003.
- (46) Liu, X. D.; Lu, B.; Iimori, T.; Nakatsuji, K.; Komori, F. *Phys. Rev. Lett.* **2007**, *98*, 66103.
- (47) Lu, B.; Liu, X. D.; Nakatsuji, K.; Iimori, T.; Komori, F. *Phys. Rev. B: Condens. Matter Mater. Phys.* **2007**, *76*, 245433.
- (48) Hou, J. G.; Yang, J. L.; Wang, H. Q.; Li, Q. X.; Zeng, C. G.; Yuan, L. F.; Wang, B.; Chen, D. M.; Zhu, Q. S. *Nature (London)* **2001**, *409*, 304.
- (49) Sekiba, D.; Shunsuke, D.; Nakatsuji, K.; Komori, F. *Surf. Sci.* **2005**, *590*, 138.
- (50) Otero, R.; Naitoh, Y.; Rosei, F.; Jiang, P.; Thostrup, P.; Gourdon, A.; Lægsgaard, E.; Stensgaard, I.; Joachim, C.; Besenbacher, F. *Angew. Chem.* **2004**, *43*, 2092.
- (51) Cicoira, F.; Miwa, J. A.; Melucci, M.; Barbarella, G.; Rosei, F. *Small* **2006**, *2*, 1266.
- (52) Cicoira, F.; Miwa, J. A.; Perepichka, D. F.; Rosei, F. *J. Phys. Chem. A* **2007**, *111*, 12674.